



OPEN

Optimization of dyes and toxic metals removal from environmental water samples by clinoptilolite zeolite using response surface methodology approach

Xinpo Sun^{1✉}, Reathab Abbass², Milad Ghoroghi^{3✉}, Indrajit Patra⁴, Ngakan Ketut Acwin Dwijendra⁵, Khusniddin Abduriddinovich Uktamov⁶ & Hadeer Jasem⁷

The present study aimed to remove crystal violet (CV), malachite green (MG), Cd(II), and Pb(II) from an aqueous solution using clinoptilolite zeolite (CZ) as an adsorbent. Response surface methodology (RSM) based on central composite design (CCD) was used to analyze and optimize the process parameters, such as pH, analyte concentration, adsorbent amount, and sonication time. Quadratic models with the coefficient of determination (R^2) of 0.99 ($p < 0.0001$) were compared statistically. The results revealed that the selected models have good precision and a good agreement between the predicted and experimental data. The maximum removal of contaminants was achieved under optimum conditions of pH = 6, sonication time of 22 min, the adsorbent amount of 0.19 g, and analyte concentration of 10 mg L⁻¹. The reusability test of the adsorbent showed that the CZ adsorbent could be used 5 times in water and wastewater treatment processes. According to the results of interference studies, the presence of different ions, even at high concentrations, does not interfere with the removal of contaminants. Applying the CZ adsorbent on environmental water samples revealed that CZ adsorbent could remove CV, MG, Cd(II), and Pb(II) in the range of 84.54% to 99.38% and contaminants present in industrial effluents. As a result, the optimized method in this study can be widely used with high efficiency for removing CV, MG, Cd(II), and Pb(II) from water and wastewater samples.

The expansion of industries and the release of industrial effluents into the environment have led to the risk of pollution around factories, surface water, and groundwaters. Various industries such as plastics, textiles, food, and cosmetics discharge effluents containing different pollutants such as organic materials and dyes into the environment¹⁻³. The most critical problem in treating dye-contained effluents is the removal of unstable dyes. In this regard, even trace amounts of dye in the water are easily visible as factors threatening aquatic life⁴⁻⁶.

Pb, Hg, Cd, Zn, Cu, and Ni are the most common heavy metals in aqueous systems. These elements are toxic to organisms at threshold concentrations. Accumulating toxins in the food chain can increase the contaminant concentration in animals at high levels of the food chain⁷⁻⁹.

¹College of Civil Engineering, Sichuan University of Science and Engineering, Zigong 643000, China. ²Medical Technical College, Al-Farahidi University, Baghdad, Iraq. ³Department of Environmental Engineering, School of Environment, College of Engineering, University of Tehran, Tehran, Iran. ⁴National Institute of Technology (NIT) Durgapur, Durgapur, West Bengal, India. ⁵Faculty of Engineering, Udayana University, Bali 80361, Indonesia. ⁶Economic Security Department, Tashkent State University of Economics, Tashkent, Uzbekistan. ⁷Medical Instrumentation Techniques Engineering Department, Al-Mustaqbal University College, Babylon, Iraq. ✉email: xinpohd@163.com; Milad.Ghoroghi@ut.ac.ir

Crystal violet (CV) and malachite green (MG) dyes are water-soluble. These two dyes are widely used in the textile, paper, printing, textile, fish farming, and silk industries. CV and MG dyes contain aromatic groups that cause allergies, dermatitis, skin irritation, cancer, and genetic mutations^{10–12}.

Several methods such as adsorption, chemical coagulation, oxidation, and membrane separation have been used to remove contaminants from industrial effluents^{13–17}.

However, choosing the best treatment technique depends on the final purpose and type of effluent. In this regard, low-cost, robust, and more efficient techniques are highly beneficial for treating wastewater without endangering human health or damaging the environment. Adsorption is one of the low-cost and efficient techniques in pollution removal^{18,19}.

Recently, the use of inexpensive adsorbents has drawn the attention of many researchers. Inexpensive adsorbents are those with a high abundance, availability, and low preparation cost. These adsorbents mainly include sawdust, Guar gum, clay, activated carbon, and clinoptilolite zeolite (CZ), which effectively adsorb dyes and heavy metals^{20–24}. CZ has a 3D structure whose typical molecular structure is $\text{Na}_6[(\text{AlO}_2)_6(\text{SiO}_2)_{30} \cdot 4\text{H}_2\text{O}]$. CZ is highly beneficial for practical applications due to its pores, high thermal resistance, and chemical neutral base structure. This adsorbent can easily absorb some heavy metal cations such as lead, zinc, cadmium, nickel, and dyes from an aqueous medium^{25,26}.

Afshin et al.²⁷ used Zeolite/ Fe_3O_4 nanocomposite to adsorb the basic blue-1 cationic dye. The obtained results showed that the efficiency of the adsorption process increases with increasing the reaction time, pH, and the adsorbent amount. In contrast, increasing the initial dye concentration diminishes adsorption efficiency significantly. The removal efficiency of 71.4% was achieved under optimum conditions of pH = 9, the reaction time of 60 min, the adsorbent amount of 3 g L^{-1} , and the initial concentration of 100 mg L^{-1} . The results revealed that Zeolite/ Fe_3O_4 nanocomposite could be used as an available, environmentally friendly, and cost-effective adsorbent for the removal of dyes from effluents of various industries.

Molla Mahmoudi et al.²⁸ used acid-treated clinoptilolite to remove methylene blue (MB) dye from an aqueous solution. The results showed that the highest dye adsorption efficiency was achieved at pH = 10, the adsorbent amount of 0.5 g L^{-1} , dye concentration of 50 mg L^{-1} , and contact time of 90 min²⁸.

Zanin et al.²⁹ assessed using natural clinoptilolite zeolite for the removal of copper(II), chromium(III), and iron(III) from wastewater. Maximum removal of 95.3% iron, 96.3% copper, and 85.1% chromium was achieved at 25°C and pH = 4. The results disclosed that clinoptilolite zeolite is highly efficient as an adsorbent for treating the wastewater of the printing industry²⁹.

The general method to study the factors affecting the process is to change one factor individually, i.e., one factor at a time (OFAT). In this technique, the effect of each factor is studied individually, neglecting the fact that the combination of different factors can intensify or neutralize each other's effects^{30–32}. Today, statistical and engineering methods such as the response surface methodology (RSM) are used to solve this issue³³. This method needs fewer tests and is suitable for multifactor systems. In this method, the relationship of various factors is considered. In this case, the linear or quadratic effects of the tested variables will create the desired graphs and the appropriate model. Consequently, each variable's appropriate values and relevance can be easily determined and predicted^{34,35}.

Therefore, the present study explored CV, MG, Cd(II), and Pb(II) removal from contaminated water by CZ as a low-cost adsorbent. The RSM optimized the removal conditions, including adsorbent amount, analyte concentration, sorption time, and pH. Moreover, the adsorbent's performance in environmental water samples and its reusability were investigated.

Materials and methods

Materials and instruments. All materials used in this study, including crystal violet dye ($\lambda_{\text{max}} = 585 \text{ nm}$, $\text{C}_{25}\text{H}_{30}\text{ClN}_3$), malachite green dye ($\lambda_{\text{max}} = 615 \text{ nm}$, $\text{C}_{23}\text{H}_{25}\text{ClN}_2$), cadmium nitrate tetrahydrate ($\text{Cd}(\text{NO}_3)_2 \cdot 4\text{H}_2\text{O}$), and Lead nitrate ($\text{Pb}(\text{NO}_3)_2$), were purchased from Merck and Aldrich with the laboratory purity and grade. Clinoptilolite zeolite (CZ) was supplied from Afrazand Mineral Company. The stock solution of 1000 mg L^{-1} was prepared from each analyte separately. Solutions of NaOH (0.1 M) and HCl (0.1 M) were used to adjust the pH, and measuring was done using a pH meter (Mettler Toledo). An ultrasonic bath (WUCD10H, 30 kHz, 665 W) was used to mix the adsorbent and the contaminant. Atomic absorption spectroscopy (AAS) model PG990 and UV-Vis spectrophotometer model Philips PU 8700 were used to measure the concentration of metal ions and dyes, respectively. Scanning Electron Microscope (SEM), X-ray diffraction (XRD), and Brunauer–Emmett–Teller (BET) techniques were used to characterize the CZ.

Preparation of clinoptilolite zeolite (CZ). Clinoptilolite zeolite (CZ) samples were crushed after preparation and sieved to mesh size 40 using ASTM standard sieves. Before preparing the adsorbent for the experiment and removing its fine particles and salts, CZ was first washed with distilled water. This process was performed in triplicate. The adsorbent was oven-dried at above 100°C for 24 h to remove moisture from its internal pores and provide space to enter contaminants from the effluent to the adsorbent.

Batch experiments. Ultrasonic-assisted adsorption experiments were conducted in batch mode. For this purpose, 0.19 g adsorbent was added to a 250 mL Erlenmeyer flask containing 100 mL of the contaminant. The pH of the solution was adjusted to 6 using a pH meter. The Erlenmeyer flask was then placed in an ultrasonic bath for 22 min with a frequency of 25 kHz. The solid and liquid phases were separated using a centrifuge at 3000 rpm for 10 min. The solution was then passed through a filter paper. Finally, the residual concentrations of dye and metal ions in the solution were measured by UV/Vis spectrophotometer and atomic absorption spec-

troscopy, respectively. The removal percentage of contaminants was calculated according to Eq. (1). All experiments were performed at 25 °C.

$$\%R = \frac{C_0 - C_e}{C_0} \times 100 \quad (1)$$

where R was the removal percentage, C_0 (mg L^{-1}) was the analyte concentration in the initial solution, and C_e (mg L^{-1}) was the equilibrium concentration after contact with the adsorbent³⁶.

Experimental design. The RSM is a robust tool for statistical modeling conducted using the least number of experiments according to the experimental design. Today, RSM is widely used to optimize process variables. This technique is based on a nonlinear multivariate model consisting of an experimental design to provide sufficient and reliable response values, provide a mathematical model that best fits the data obtained from the experimental design, and determine the optimum value of the independent variables^{37,38}. There are different types of RSM, and this statistical method can be used in different ways. Central composite design (CCD) is one of the most popular models, which is a quadratic design based on fractional three-level factorial designs. This method can estimate the value of the parameters in a quadratic model, create the required designs, and calculate the value of the lack-of-fit parameter. This design allows the responses to be modeled by fitting a second-order polynomial, which can be expressed as Eq. (2).

$$Y = \beta_0 + \sum_{i=1}^k \beta_i X_i + \sum_{i=1}^k \beta_{ii} X_i^2 + \sum_{i < j}^k \sum_{j=1}^k \beta_{ij} X_i X_j + \epsilon \quad (2)$$

where β_0 is the regression coefficient, β_i is the linear effect, β_{ii} is the quadratic effect, β_{ij} is the linear interaction, k is the number of variables, x_i and x_j are the encoded values of variables, i is the linear coefficient, j is the quadratic coefficient, Y is the response (removal percentage), and ϵ is the residual error. The number of points (N) can be obtained from Eq. (3).

$$N = K + 2K + C_p \quad (3)$$

where K is the number of variables and C_p is the number of central points.

Results and discussion

Characterization of the clinoptilolite zeolite (CZ). SEM analysis was used to study the morphological features of CZ. Figure 1a shows the SEM image of CZ. It can be seen that the sample has an irregular perforated crystalline texture, which is layered on top of each other. Such a pattern provides suitable adsorption sites for the absorption of different species of contaminants.

The sample structure was studied by XRD analysis. XRD analysis was assessed in the 2θ range of 5° and 50° . The XRD diagram (Fig. 1b) of clinoptilolite revealed diffraction peaks at 2θ values of 9.7° , 22.4° , 26.8° , 30.2° , and 32.8° , which correspond to biotite (Bi), Clinoptilolite (Clp), quartz (Qtz), feldspar (Fel), and dolomite (Dol), respectively. These results are consistent with the XRD data of clinoptilolite reported in the literature^{39,40}.

CZ structure information was determined by N_2 gas adsorption analysis at 77.3 K in the relative pressure range (P/P_0) of 0.098. The test sample was degassed for 2 h at 120°C . The values of specific surface area, total volume of pores, and average diameter of pores were measured by the standard BET method. According to this analysis, the surface area, micropore volume, and pore diameter were $15.01 \text{ m}^2 \text{ g}^{-1}$, $0.1947 \text{ cm}^3 \text{ g}^{-1}$, and $0.0174 \mu\text{m}$, respectively (Fig. 1c).

Central composite design (CCD). In the present study, the parameters affecting the process were optimized using the CCD. The design of four parameters, including sonication time, adsorbent amount, pH, and contaminant concentration, was studied at five levels. The factors and experimental results are shown in Table 1. Experimental results and predicted results are shown in Table S1.

Statistical analysis was conducted with version 10 of Design-Expert Software (DX 10). The response function and the obtained experimental data were fitted using the quadratic and linear effects of the independent variables and regression coefficients. Also, the analysis of variance (ANOVA) results were used to estimate significant differences between variables and their interaction. Regression coefficients and ANOVA of the quadratic equation of polynomials in removing contaminants are summarized in Tables S2 and S3. According to Tables S2 and S3, all linear effects (A, B, C, and D) and all quadratic effects (A^2 , C^2 , B^2 , and D^2) were significant with a 95% confidence level. The F-value of all models was very high (at 95% significance), confirming the validity of the models. High values of R^2 (more than 99% for all analytes) indicated good agreement of the model with experimental data. There was no significant difference between R^2 and R^2 -Adj values, indicating a high correlation between the experimental and predicted results. Also, the insignificance of the lack of fit ($P > 0.05$) revealed the good fitness of the predicted model. Adequate precision was employed to evaluate the adequacy of the models. The adequate precision is determined by comparing the predicted response values at the design points with the average prediction error. The adequate precision in this study was more than 4 for all models, suggesting that the model was acceptable. The two-level response of the second-order polynomial equation for CV, MG, Cd(II), and Pb(II) is shown in Eqs. 4–7, respectively.

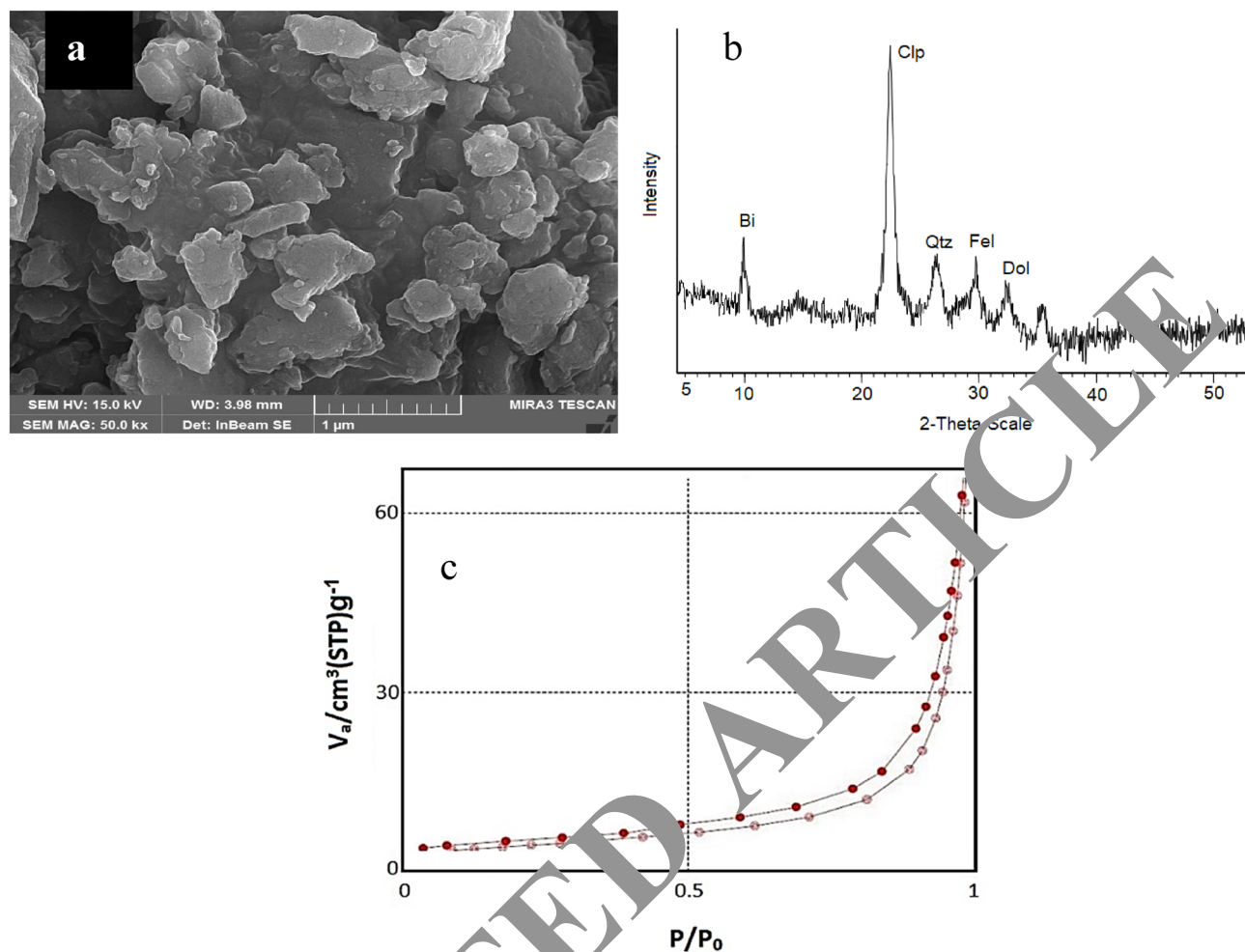


Figure 1. (a) SEM image and (b) XRD pattern and (c) adsorption-desorption isotherm of CZ.

$$\begin{aligned} \% \text{Removal (CV)} = & +87.13 + 10.630A + 8.68B - 9.56C + 8.69D \\ & + 0.19AB - 0.81AC - 0.24AD - 0.53BC + 1.15BD \\ & + 1.03CD - 7.80A^2 - 10.31B^2 - 4.11C^2 - 5.48D^2 \end{aligned} \quad (4)$$

$$\begin{aligned} \text{oval (MG)} = & +90.41 + 11.28A + 11.84B - 10.46C + 7.21D \\ & + 1.35AB - 1.89AC - 0.09AD - 2.10BC - 0.38BD \\ & - 0.19CD - 11.10A^2 - 13.16B^2 - 6.30C^2 - 5.10D^2 \end{aligned} \quad (5)$$

$$\begin{aligned} \% \text{Removal (Cd(II))} = & +87.25 + 8.98A + 7.49B - 9.40C + 6.21D + 1.08AB \\ & + 0.50AC + 1.41AD - 0.64BC - 0.07BD \\ & + 1.18CD - 6.06A^2 - 8.41B^2 - 5.49C^2 - 5.65D^2 \end{aligned} \quad (6)$$

$$\begin{aligned} \% \text{Removal (Pb(II))} = & +91.72 + 7.12A + 8.74B - 8.64C + 3.81D + 1.39AB \\ & - 0.11AC + 0.54AD + 0.53BC - 0.06BD \\ & + 0.62CD - 6.97A^2 - 7.99B^2 - 5.98C^2 - 5.60D^2 \end{aligned} \quad (7)$$

In these equations, A, B, C, and D were the adsorbent amount (g), pH of the solution, analyte concentration ($mg L^{-1}$), and sonication time (min), respectively. The next step in evaluating the proposed models is to analyze the residual graphs. Figure 2a–d show a good correlation between the experimental values and the predicted values. Regression models had a high R^2 , indicating the validity of the selected models.

Residuals, which are the difference between the experimental and predicted removal efficiency, are useful for evaluating the importance of a model. Figure 3a–d shows the normal probability compared to the residuals. As can be seen, the residual points create a straight line. These plots confirmed the applicability of the model.

Variables	Unit	Range and levels						
		- α	-1	0	+1	+ α		
A—CZ amount	g	0.05	0.10	0.15	0.20	0.25		
B—pH of the solution	-	2	4	6	8	10		
C—Analyte concentration	mg L ⁻¹	5	10	15	20	25		
D—Sonication time	min	5	10	15	20	25		
Run	A	B	C	D	%R _{CV}	%R _{MG}	%R _{Cd(II)}	%R _{Pb(II)}
1	-1	-1	-1	-1	39.19	30.00	49.36	54.41
2	1	-1	-1	-1	65.77	55.74	64.12	71.18
3	-1	-1	1	-1	24.19	20.49	31.39	38.87
4	1	-1	1	-1	40.23	32.74	43.14	54.54
5	-1	1	-1	-1	56.54	54.93	66.65	65.54
6	1	1	-1	-1	78.54	87.88	86.65	86.73
7	-1	1	1	-1	35.77	36.05	40.35	53.28
8	1	1	1	-1	56.68	58.86	60.18	67.77
9	-1	-1	-1	1	54.91	45.3	58.28	64.48
10	1	-1	-1	1	75.35	70.6	75	72.27
11	-1	-1	1	1	40.65	32.26	42.26	42.61
12	1	-1	1	1	59.58	51.02	60.42	59.34
13	-1	1	-1	1	75.39	77.7	72.37	75.00
14	1	1	-1	1	96.45	97.7	92.95	93.63
15	-1	1	1	1	70.97	48.24	52.39	62.19
16	1	1	1	1	78.2	72.20	78.28	78.50
17	-2	0	0	0	35.87	25.78	46.96	50.06
18	2	0	0	0	68.23	68.23	83.19	80.36
19	0	0	-2	0	92.63	87.97	85.69	87.16
20	0	0	0	0	52.74	44.40	49.01	51.15
21	0	-2	0	0	29.45	15.53	40.27	44.25
22	0	2	0	0	66.27	61.96	71.07	78.02
23	0	0	0	-2	50.19	56.31	53.85	63.93
24	0	0	0	2	84.16	85.69	79.64	77.47
25	0	0	0	0	85.93	89.44	85.75	93.07
26	0	0	0	0	88.28	90.97	86.94	89.53
27	0	0	0	0	87.18	91.64	86.39	91.56
28	0	0	0	0	87.05	88.97	87.83	89.7
29	0	0	0	0	88.85	91.83	89.47	92.36
30	0	0	0	0	85.52	89.66	87.17	94.12

Table 1. The design of CCD.

The normality of the data was studied with a plot of residuals' normal probability. The normal plot of residuals in Fig. 4a–d indicates a random scatter of residuals compared to the expected values, indicating a satisfactory model fit.

The three-dimensional (3D) plots. To assess the interaction of all four parameters, three-dimensional (3D) graphs were designed for the predicted responses based on the quadratic model. Response surface graphs are often employed to estimate removal efficiencies for different values of experimental parameters. Using the CZ adsorbent, this study investigated and optimized the parameters affecting the removal efficiency of CV, MG, Cd(II), and Pb(II). Three-dimensional diagrams of the simultaneous effect of adsorbent amount (A), pH (B), contaminant concentration (C), and sonication time (D) are shown in Fig. 5a–d.

Figure 5a displays the simultaneous effect of the adsorbent amount and the pH of the solution on the amount of CV dye removal. The results show that the percentage of CV dye removal has increased with increasing the adsorbent amount to the extent that the intensity of changes decreases. The explanation for this increase is that with increasing the adsorbent amount, the number of active sites for the absorption of contaminants increases. According to the results, the optimum value for the adsorbent amount was 0.19 g. These results are consistent with Bagheri et al.⁴¹, who studied the removal of lead and cadmium from aqueous solutions. In this study, rGO-Fe₀/Fe₃O₄-PEI nanocomposite was used as the adsorbent. Next, the effect of different variables such as the adsorbent dosage, ultrasound time, dye concentration, and pH on the amount of dye removal was examined. This study showed that the amount of dye removal increases with increasing the adsorbent amount⁴¹. Asfaram et al. (2015) employed ZnS:Cu nanoparticles loaded on activated carbon (ZnS:Cu-NP-AC) as an adsorbent for

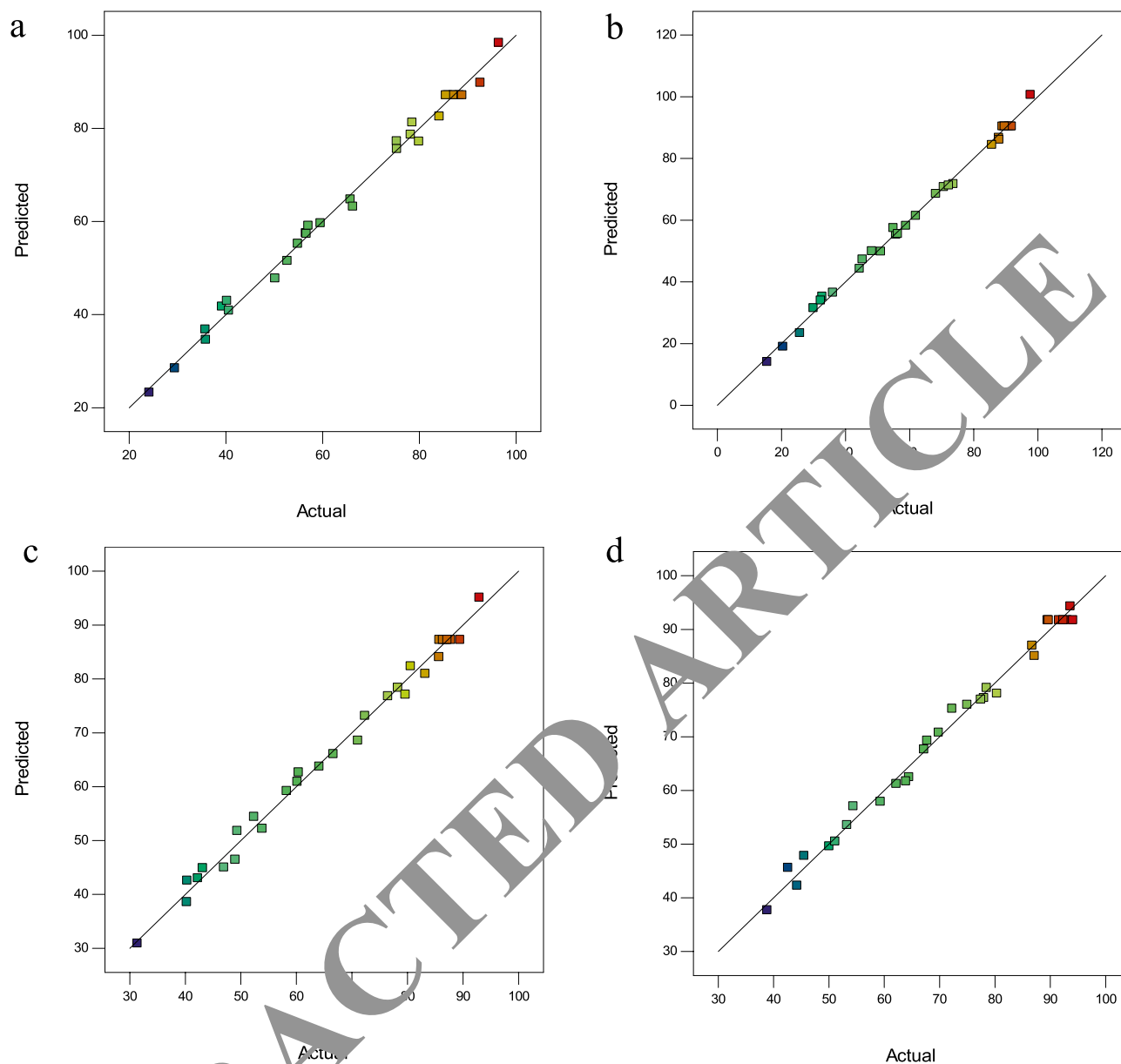


Figure 2. Predicted versus actual removal efficiency plots (a) CV, (b) MG, (c) Cd(II), and (d) Pb(II).

the removal of Auramine-O (AO) dye from an aqueous solution. They found that the percentage of contaminant removal increases with increasing the adsorbent amount⁴².

Figure 5a illustrates the effect of pH on CV removal efficiency. The 3D plot shows that the dye removal percentage increases with the pH. CV is a cationic dye, and since the adsorbent surface becomes positive in an acidic environment, less adsorption occurs on the adsorbent surface due to the electrostatic repulsion between the positive charges of the dye and the adsorbent. Hence, the removal rate of CV in acidic environments is low. Moreover, the percentage of lead removal also increased with increasing pH, and the maximum lead removal was achieved at pH 6 (Fig. 5d). Since the pH_{zpc} of CZ is 3, there is a positive charge on the surface of CZ at pHs below 3^{43–45}. Therefore, at pHs lower than 3, the electrostatic repulsion between the positively charged metal and the positive charge on the adsorbent surface would reduce the lead removal rate. On the other hand, with increasing pH, the adsorbent surface becomes more negative; therefore, the adsorption of metal cation increases. As the pH increases, the metal ion removal efficiency initially increases and then decreases. The reason is that at pHs above 6, lead hydroxide ($Pb(OH)_2$) and cadmium hydroxide ($Cd(OH)_2$) are formed, which are insoluble and precipitate. Similar results have been reported by Palma-Anaya et al., Shi et al., and Rahimi et al.^{46–48}.

The simultaneous effect of MG concentration and sonication time on the percentage of MG removal is shown in Fig. 5b. According to Fig. 5b, the removal efficiency decreased by increasing the dye concentration from 5 to 25 mg L⁻¹. The explanation is that the surface of nanoparticles is saturated in the presence of a higher concentration of dye molecules. Dye molecules tend to aggregate on the outer surface of nanoparticles, reducing the adsorption rate. Hence, lower dye concentrations can be easily absorbed on the adsorbent surface. Chauhan et al.⁴⁹ obtained similar results in removing bromophenol blue (BB) dye. The effect of various parameters such

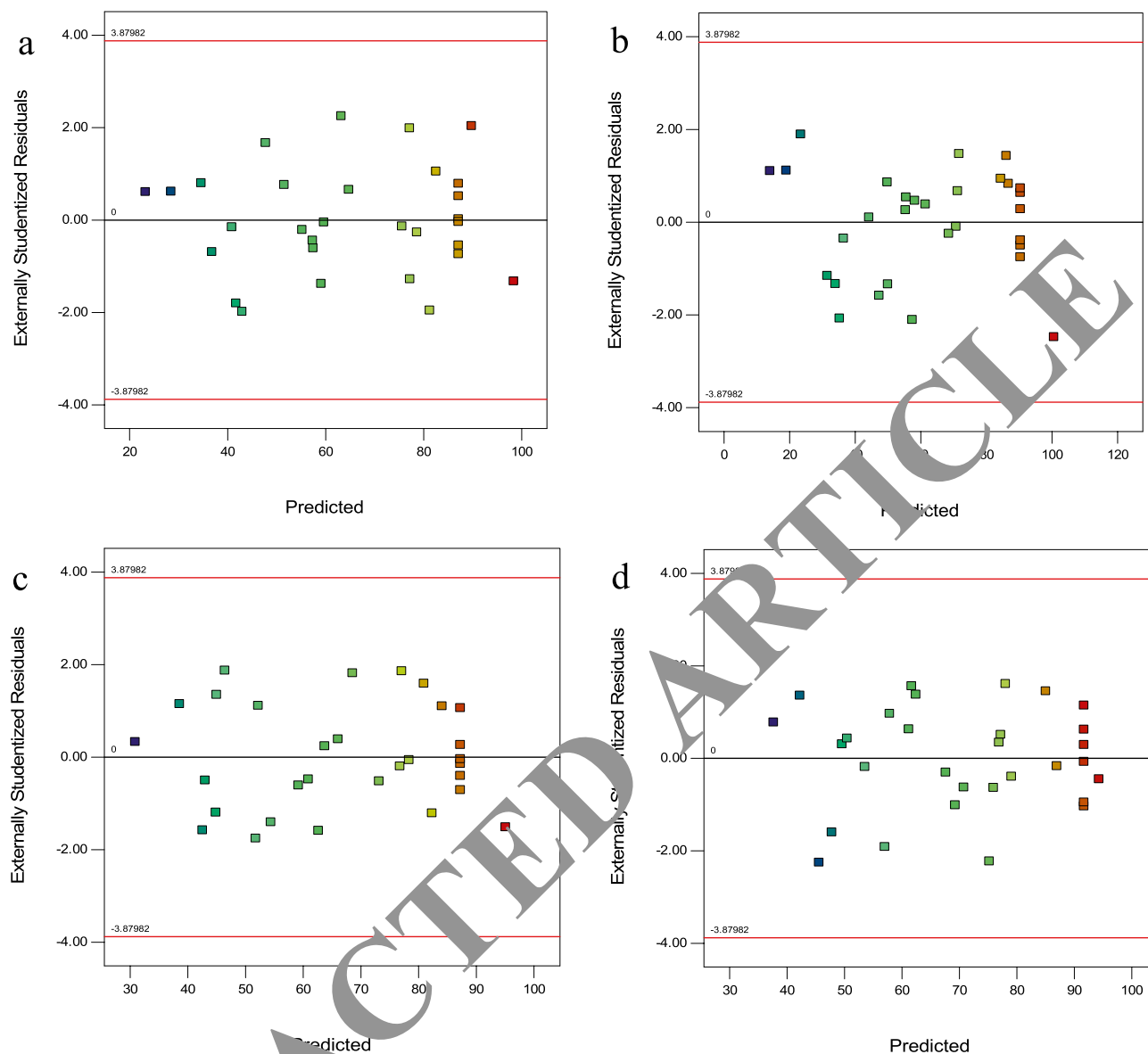


Figure 3. Plot of residuals versus predicted (a) CV, (b) MG, (c) Cd(II), and d) Pb(II).

pH, response time, dosage amount, and concentration of BB on the removal rate was also investigated. The results revealed that increasing the dye concentration reduced the removal rate, which is consistent with the present study results⁴⁹. Also, Awual⁵⁰ obtained similar results in investigating dye concentration's effect on Cd(II) removal rate. This study applied the ligand-coated porous composite material as an adsorbent to remove Cd(II). According to the results, increasing the concentration of Cd(II) reduced the removal rate⁵⁰.

Figure 5c exhibits the effect of sonication time on Cd(II) removal rate. The removal efficiency generally increases with increasing contact time and reaches a constant value in the equilibrium state. Therefore, sonication time can affect the contaminant removal efficiency due to its effect on the analyte mass transfer. Sonication time was assessed from 5 to 25 min. According to the results, Cd(II) removal was first increased with increasing the sonication time. However, no significant change in removal was observed after 22 min. The explanation is that in these conditions, the contact between the adsorbent and the metal ion is high, leading to mass transfer and removing the contaminants. Khalifa et al.⁵¹ obtained similar results in the removal of Cd(II), Hg(II), and Cu(II) ions using mesoporous silica nanoparticles modified with dibenzoylmethane. Arabkhani and Asfaram⁵² obtained similar results for removing MG dye from an aqueous solution using a three-dimensional magnetic polymer aerogel. This study investigated the effect of various parameters (e.g., adsorbent amount, initial dye concentration, temperature, contact time, and pH of dye solution) on the amount of dye removal. Consistent with the present study, the results indicated that the removal percentage increased with increasing the sonication time⁵².

Process optimization. One of the main objectives of this study was to identify the optimum conditions for maximizing the removal efficiency of contaminants using the proposed mathematical model^{53,54}. For this purpose, numerical optimization was utilized to determine the desired values of each parameter and obtain the

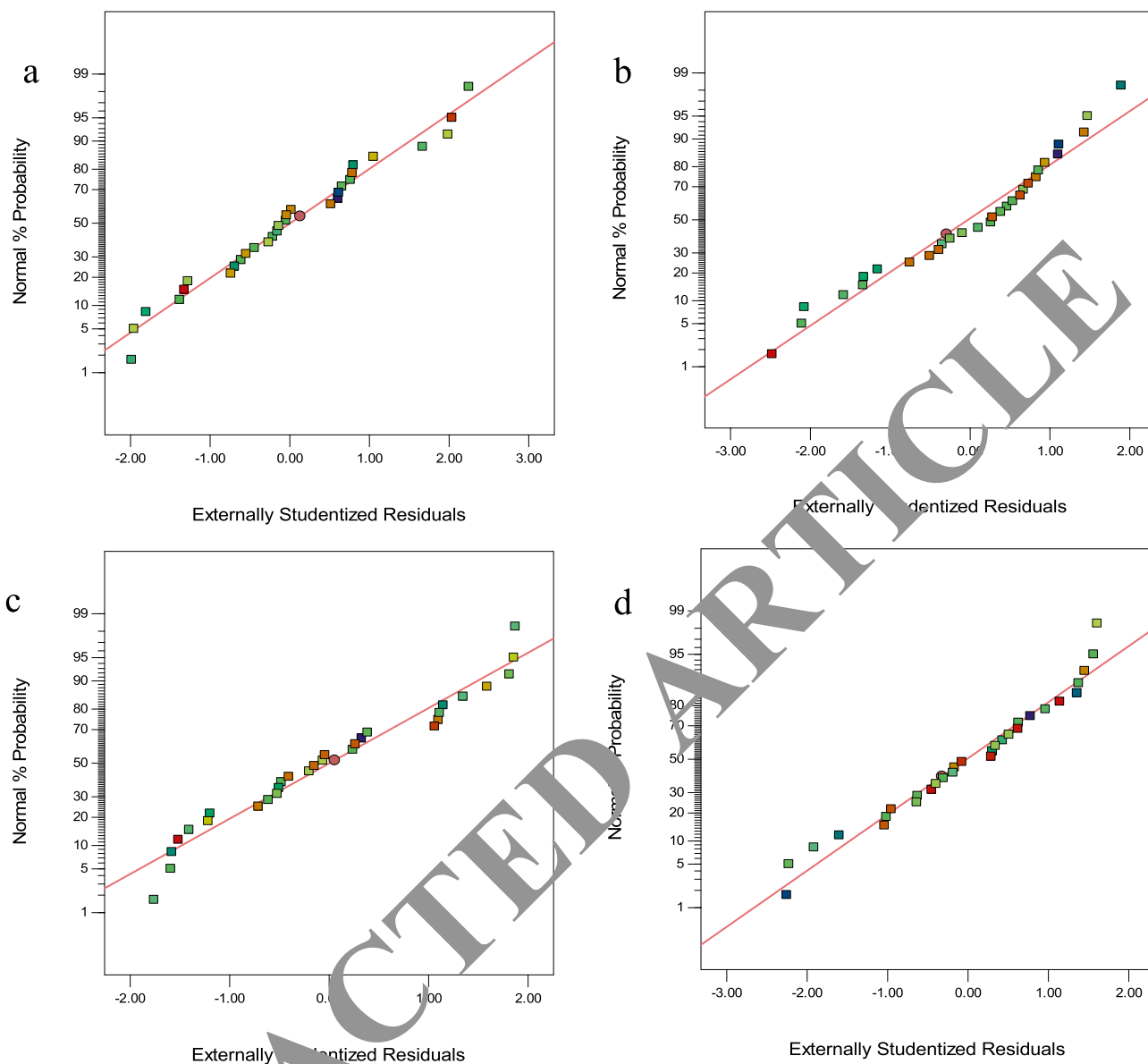


Figure 4. The normal plot of residuals (a) CV, (b) MG, (c) Cd(II), and (d) Pb(II).

maximum removal rate. The results of contaminant removal optimization are presented in Table 2. The numerical optimization results showed that the maximum removal efficiency could be achieved with an adsorbent of 0.19 g, an analyte concentration of 10 mg L^{-1} , a pH of 6, and a sonication time of 22 min. The obtained results were validated by conducting an additional experiment under optimum conditions. It was found that under optimum operating parameters, the experimental removal efficiency was more than 92.67% for all analytes, suggesting the model's predictability for use in real conditions.

Effect of interfering ions. It is often very difficult to remove the desired analytes from different matrices containing different ions. For this purpose, the effect of interfering ions of Na^+ , Mg^{2+} , Al^{3+} , Ba^{2+} , Fe^{3+} , and F^- was studied to obtain a minimum of 95% analyte adsorption signal in the presence of different anions and cations during the process. During the experiment, different ions at different concentrations were added individually to the solution containing CV, MG, Cd(II), and Pb(II), and tolerance limits were determined. Interfering ions and their tolerance limits are presented in Table 3.

The reusability of CZ. The reusability of the adsorbent is a critical aspect that makes the adsorbent effective for practical applications. Therefore, the reusability of CZ was examined under optimized conditions to remove contaminants (Fig. 6). The CZ adsorbent was separated from the solution by centrifugation at 3000 rpm (for 10 min). The adsorbent was washed with 5 mL of HNO_3 solution (0.1 M). Finally, the adsorbent was washed several times with distilled water and dried at 80°C . This process was repeated after each experiment. It was

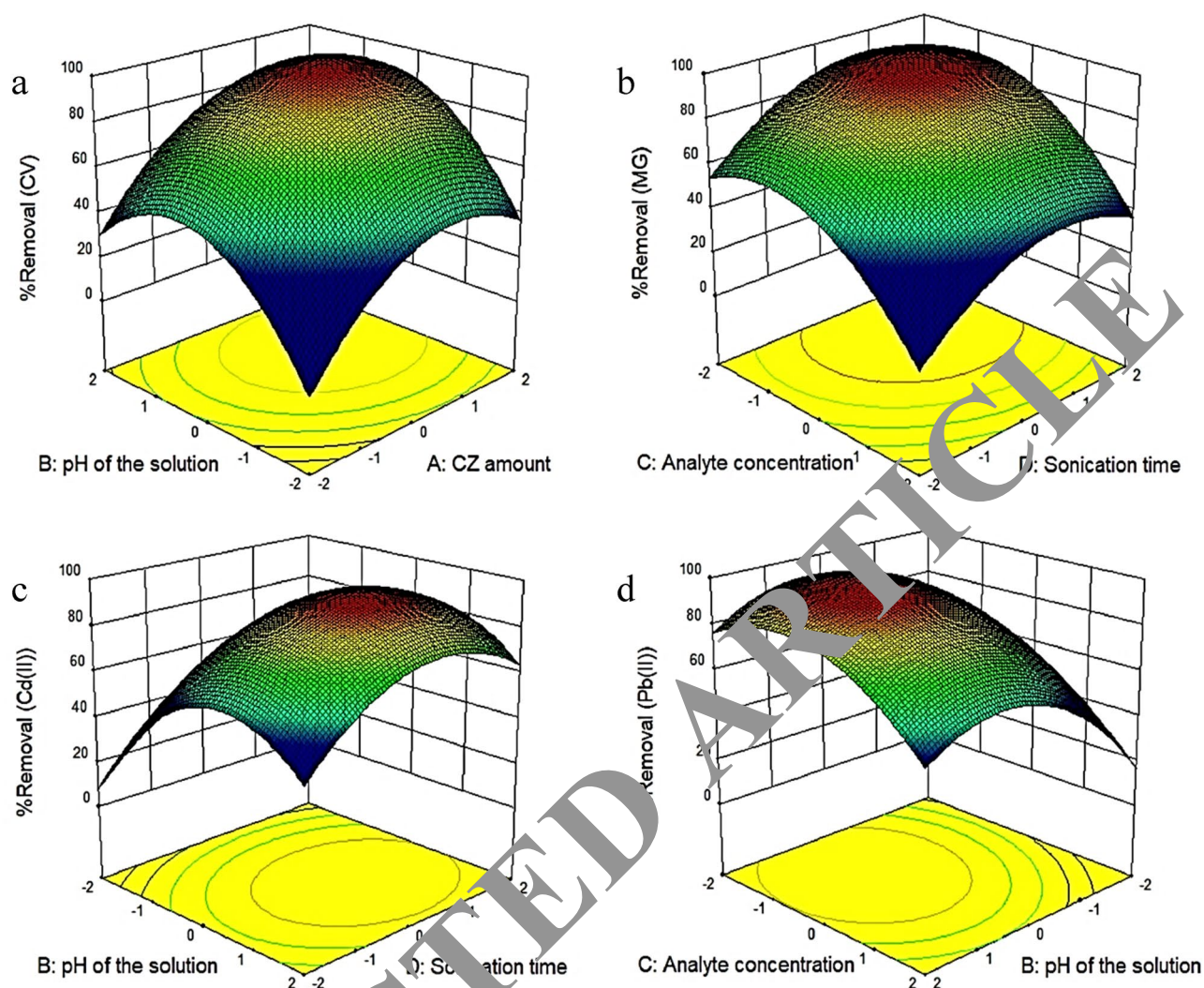


Figure 5. Three-dimensional plots of the interaction effects between variables and removal of (a) CV, (b) MG, (c) Cd(II), and (d) Pb(II).

Run	Variables				%Removal											
	A (g)	B	C (mg/L)	D (min)	CV			MG			Cd(II)			Pb(II)		
					Ex ^a	Pr ^b	E ^c	Ex ^a	Pr ^b	E ^c	Ex ^a	Pr ^b	E ^c	Ex ^a	Pr ^b	E ^c
1	0.19	6	10	22	99.15	99.82	0.67	99.69	99.75	0.06	93.37	94.25	0.88	94.22	95.89	1.67
2	0.19	6	10	22	98.82	99.82	0.510	98.79	99.75	0.96	92.67	94.25	1.58	95.26	95.89	0.63
3	0.19	6	10	22	98.75	99.82	1.07	99.20	99.75	0.55	94.46	94.25	-0.21	93.85	95.89	2.04

Table 2. Optimum conditions of removal of CV, MG, Cd(II) and Pb(II). ^aExperimental, ^bPredicted, ^cError.

observed that the removal efficiency decreased by about 10% after five consecutive runs. This result demonstrates that CZ adsorbent is reusable and stable for removing contaminants from environmental water samples.

Real sample analysis. The adsorption capacity of CZ was studied in various real water samples (e.g., tap water, well water, river water, and fish farm) to confirm the system's efficiency. In this analysis, the proposed water samples with specific concentrations of contaminants were spiked under optimum conditions. After performing the relevant experiment, the efficiency of the CZ adsorbent was calculated using the given method (Table 4). Therefore, the adsorbent can effectively remove CV, MG, Cd(II), and Pb(II) from any wastewater.

Comparison CZ adsorbent with other adsorbents. According to the results, CZ adsorbent can be used as an adsorbent in the removal of CV, MG, Cd(II) and Pb(II). Table 5 shows some recent studies on vari-

Interference	Tolerance (mg L ⁻¹)	%R _{CV}	%R _{MG}	%R _{Cd(II)}	%R _{Pb(II)}
Fe ³⁺	0	97.23	98.49	94.47	93.91
	50	96.18	96.80	92.17	89.04
	100	91.58	92.05	87.46	86.58
	150	85.16	86.57	82.73	81.93
Na ⁺	0	96.07	95.52	90.84	91.81
	50	93.77	93.46	89.76	89.50
	100	91.14	92.92	87.74	85.79
	150	86.75	88.37	86.40	82.43
Mg ²⁺	0	94.29	92.85	88.69	87.20
	50	92.00	89.73	85.19	85.37
	100	88.02	87.35	83.04	83.64
	150	85.17	84.08	81.28	80.59
F ⁻	0	98.52	99.35	93.67	94.21
	50	95.04	97.69	91.09	90.67
	100	89.28	92.49	87.83	88.00
	150	84.96	85.69	84.78	84.58
Ba ²⁺	0	96.46	98.41	92.68	91.56
	50	94.24	96.82	88.37	88.29
	100	91.30	91.99	85.49	84.81
	150	85.34	87.08	81.36	82.14
Al ³⁺	0	96.45	97.29	93.46	92.71
	50	93.51	93.87	90.71	89.83
	100	90.49	88.06	87.35	86.64
	150	86.83	85.43	84.99	82.71

Table 3. Effect of interfering ions on the removal of MG, MB, Cd(II) and Pb(II).

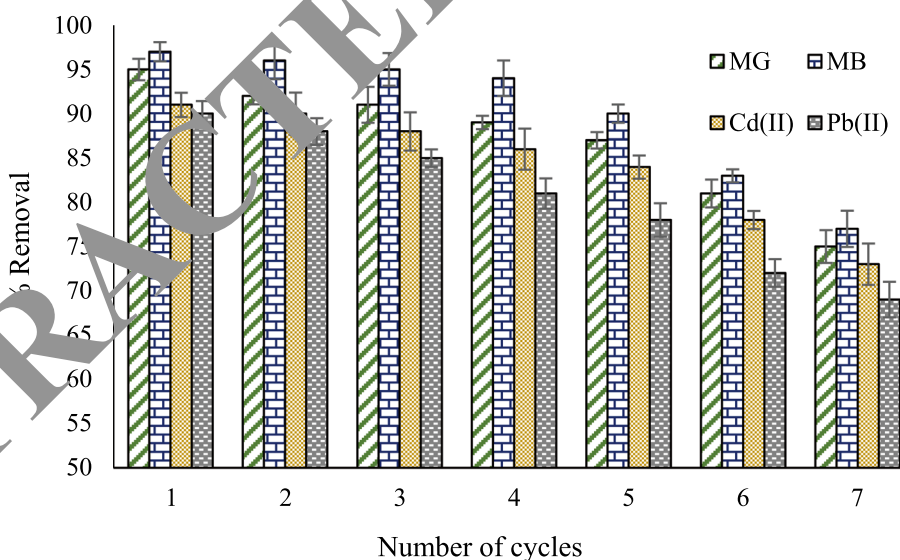


Figure 6. The reusability of CZ in the removal of pollutants under optimized parameters.

Real samples	%R _{CV} ± RSD	%R _{MG} ± RSD	%R _{Cd(II)} ± RSD	%R _{Pb(II)} ± RSD
Tap water	98.14 ± 2.9	99.38 ± 2.5	94.05 ± 3.1	93.25 ± 2.7
Well water	94.68 ± 3.2	93.58 ± 4.2	84.54 ± 3.2	85.37 ± 3.3
River water	95.16 ± 3.5	95.37 ± 3.1	86.41 ± 2.9	90.43 ± 2.6
Fish farm	96.02 ± 4.1	95.25 ± 3.9	89.11 ± 3.5	90.49 ± 2.8

Table 4. Removal of CV, MG, Cd(II) and Pb(II) in real samples.

Adsorbent	Analyte	Adsorbent dosage	Concentration	pH	Time	Removal/adsorption capacity	References
Chitosan	CV	1 g	77 mg L ⁻¹	7	140 min	72%	⁵⁵
Chitosan/nanodiopside	CV	0.007 g	20 mg L ⁻¹	7.5	25 min	99%	⁵⁶
Nanozeolite-X	CV	0.26 g	13 mg L ⁻¹	8	6 min	97.60%	⁵⁷
CZ adsorbent	CV	0.19 g	10 mg L ⁻¹	6	22 min	99.15%	This work
ZIF-8 ^a	MG	0.05 g	25 mg L ⁻¹	7	90 min	95%	⁵⁸
CuO-NPs-AC ^b	MG	0.02 g	30 mg L ⁻¹	10	4.5 min	100%	⁵⁹
Zr-SBA-15 ^c	MG	6.66 mg	5.48 mg L ⁻¹	7.15	4.78 min	140.61 mg g ⁻¹	⁶⁰
CZ adsorbent	MG	0.19 g	10 mg L ⁻¹	6	22 min	99.69%	This work
Hematite	Cd(II)	40 g	44.88 μmol L ⁻¹	9.2	2 h	98%	⁶¹
Polyaniline	Cd(II)	0.75 g	20 mg L ⁻¹	6	35 min	430 mg g ⁻¹	⁶²
							Coated on sawdust
Zeolite X	Cd(II)	0.4 g	20 mg L ⁻¹	7.5	30 min	99.96%	⁶³
CZ adsorbent	Cd(II)	0.19 g	10 mg L ⁻¹	6	22 min	94.46%	This work
Tobacco stems	Pb(II)	0.8 g	10 mg L ⁻¹	5	120 min	94.37%	⁶⁴
Pomegranate peel	Pb(II)	2.5 g	40 mg L ⁻¹	5.6	2 h	94.37%	⁶⁵
DgPmPDA@GO ^d	Pb(II)	120 mg	50 mg L ⁻¹	6	120 min	98%	⁶⁶
CZ adsorbent	Pb(II)	0.19 g	10 mg L ⁻¹	6	22 min	95.26%	This work

Table 5. Comparison of the CZ adsorbent with other adsorbents for removal CV, MG, Cd(II) and Pb(II). ^aZelitic imidazole framework-8, ^bMn-doped CuO-Nanoparticle loaded on activated carbon, ^cZirconium-containing mesostructured SBA-15 silica, ^dDextrin-g-poly(1,2-ethylenediamine) (DgPmPDA) and graphene oxide (GO).

ous adsorbents in the removal of CV, MG, Cd(II) and Pb(II). CZ adsorbent showed the ability to remove CV, MG, Cd(II) and Pb(II) in a short time with high efficiency. Also, the proposed method has a smaller number of experiments than other methods in the literature, which results in less consumption of adsorbent and time. As a result, CZ adsorbent showed satisfactory performance in removing CV, MG, Cd(II) and Pb(II) from environmental water samples.

Conclusion

This study applied CZ as an adsorbent to efficiently remove CV, MG, Cd(II), and Pb(II) from the environmental water samples. The synthesized adsorbent was characterized using various analyses. The surface area, micropore volume, and pore diameter were 15.01 m² g⁻¹, 0.1947 cm³ g⁻¹, and 0.0174 μm, respectively. CCD-based RSM was used to optimize, model, and predict responses. The optimal conditions of the proposed method for the removal process were 0.19 g of adsorbent, 22 min of ultrasonic time, 10 mg L⁻¹ contaminant concentration, and pH 6, respectively. Environmental water samples such as tap water, well water, river water, and fish farm were also studied. The results revealed the removal of more than 84.54% of contaminants in different samples. Sensitivity analysis showed that CZ adsorbent could be used up to 5 times efficiently to remove contaminants. The interference studies also showed that different ions do not affect the removal of CV, MG, Cd(II), and Pb. As a general result, the proposed method using CZ adsorbent has a good potential to remove toxic contaminants from water and wastewater samples effectively.

Data availability

The authors declare that data supporting the findings of this study are available within the paper [and its supplementary information files].

Received: 28 April 2022; Accepted: 28 July 2022

Published online: 02 August 2022

References

- Brinza, L., Maftai, A. E., Tascu, S., Brinza, F. & Neamtu, M. Advanced removal of Reactive Yellow 84 azo dye using functionalised amorphous calcium carbonates as adsorbent. *Sci. Rep.* **12**(1), 1–15 (2022).
- Kumar, A. *et al.* Bio-inspired and biomaterials-based hybrid photocatalysts for environmental detoxification: A review. *Chem. Eng. J.* **382**, 122937 (2020).
- Fang, X. *et al.* Employing extreme value theory to establish nutrient criteria in bay waters: A case study of Xiangshan Bay. *J. Hydrol.* **603**, 127146 (2021).
- Aljumaily, M. M. *et al.* Modification of poly(vinylidene fluoride-co-hexafluoropropylene) membranes with DES-functionalized carbon nanospheres for removal of methyl orange by membrane distillation. *Water* **14**(9), 1396 (2022).
- Tian, X. *et al.* Removal of both anionic and cationic dyes from wastewater using pH-responsive adsorbents of L-lysine molecular-grafted cellulose porous foams. *J. Hazard. Mater.* **426**, 128121 (2022).
- Shojaei, S., Nouri, A., Baharinikoo, L., Farahani, M. D. & Shojaei, S. Removal of the hazardous dyes through adsorption over nanozeolite-X: Simultaneous model, design and analysis of experiments. *Polyhedron* **196**, 114995 (2021).

7. Salami, H. A. *et al.* Towards achieving food security in Nigeria: A fuzzy comprehensive assessment of heavy metals contamination in organic fertilizers. *Curr. Res. Agric. Sci.* **8**(2), 110–127 (2021).
8. Liu, W. *et al.* Effective extraction of Cr(VI) from hazardous gypsum sludge via controlling the phase transformation and chromium species. *Environ. Sci. Technol.* **52**(22), 13336–13342 (2018).
9. Tair, R. & Eduin, S. Heavy metals in water and sediment from Liwagu River and Mansahaban River at Ranau Sabah. *Malays. J. Geosci.* **2**(2), 26–32 (2018).
10. Talukder, M. E. *et al.* Ag nanoparticles immobilized sulfonated polyethersulfone/polyethersulfone electrospun nanofiber membrane for the removal of heavy metals. *Sci. Rep.* **12**(1), 1–16 (2022).
11. Shi, C., Wu, Z., Yang, F. & Tang, Y. Janus particles with pH switchable properties for high-efficiency adsorption of PPCPs in water. *Solid State Sci.* **119**, 106702 (2021).
12. Bai, B., Rao, D., Chang, T. & Guo, Z. A nonlinear attachment-detachment model with adsorption hysteresis for suspension-colloidal transport in porous media. *J. Hydrol.* **578**, 124080 (2019).
13. Zhang, L. *et al.* The performance of electrode ultrafiltration membrane bioreactor in treating cosmetics wastewater and its anti-fouling properties. *Environ. Res.* **206**, 112629 (2022).
14. Wirnkor, V. A. *et al.* Petroleum hydrocarbons and heavy metals risk of consuming fish species from Oguta lake, Imo State, Nigeria. *J. Chem. Health Risks* **11**(1), 1–15 (2021).
15. Lin, J. Y., Mahasti, N. N. & Huang, Y. H. Recent advances in adsorption and coagulation for boron removal from wastewater: A comprehensive review. *J. Hazard. Mater.* **407**, 124401 (2021).
16. Pourabadeh, A. *et al.* Experimental design and modelling of removal of dyes using nano-zero-valent iron: simultaneous model. *Int. J. Environ. Anal. Chem.* **100**(15), 1707–1719 (2020).
17. Sharma, G. *et al.* Atrazine removal using chitin-cl-poly (acrylamide-co-itaconic acid) nanohydrogel: Isotherms and pH responsive nature. *Carbohydr. Polym.* **241**, 116258 (2020).
18. Tran, T. V. *et al.* Effective mitigation of single-component and mixed textile dyes from aqueous media using recyclable graphene-based nanocomposite. *Environ. Pollut. Res.* **29**, 1–22 (2022).
19. Alinezhad, H., Fakhimi Abarghouei, M., Tajbakhsh, M. & Niknam, K. Application of MB3-TEPA and morpholine grafted NaY zeolite as CO₂ capture. *Iran. J. Chem. Chem. Eng.* **40**(2), 581–592 (2021).
20. Ali, J. *et al.* A new biosource for synthesis of activated carbon and its potential use for removal of methylene blue and eriochrome black T from aqueous solutions. *Ind. Crops Prod.* **179**, 114676 (2022).
21. Bani-Atta, S. Potassium permanganate dye removal from synthetic wastewater using a novel, low-cost adsorbent, modified from the powder of *Foeniculum vulgare* seeds. *Sci. Rep.* **12**(1), 1–13 (2022).
22. Zouaoui, E. H., Djamel, N. & Amokarane, S. High-pressure CO₂ adsorption onto NaX zeolite: Effect of Li⁺, K⁺, Mg²⁺, and Zn²⁺ and equilibrium isotherms study. *Iran. J. Chem. Chem. Eng.* **40**(4), 1197–1215 (2021).
23. Al-Ghouti, M. A., Da'ana, D., Abu-Dieyeh, M. & Khraishel, M. Adsorptive removal of mercury from water by adsorbents derived from date pits. *Sci. Rep.* **9**(1), 1–15 (2019).
24. Sharma, G. *et al.* Guar gum and its composites as potential materials for diverse applications: A review. *Carbohydr. Polym.* **199**, 534–545 (2018).
25. Noori, M., Tahmasebpoor, M. & Foroutan, P. Enhanced adsorption capacity of low-cost magnetic clinoptilolite powders/beads for the effective removal of methylene blue: Adsorption and desorption studies. *Mater. Chem. Phys.* **278**, 125655 (2022).
26. Slota, E. *et al.* The use of H-form clinoptilolite to preconcentrate trace amounts of Nd(III) from aqueous solution under dynamic conditions. *Microporous Mesoporous Mater.* **311**, 111339 (2022).
27. Afshin, S. *et al.* Removal of basic Blue-41 dye from water by stabilized magnetic iron nanoparticles on clinoptilolite zeolite. *Rev. Chim.* **71**(2), 218–229 (2020).
28. Molla Mahmoudi, M., Naderi, A., Ghelil Aremoomand, H. R. & Mahvi, A. H. Adsorption of cationic dye textile wastewater using clinoptilolite: Isotherm and kinetic studies. *J. Text. Inst.* **110**(1), 74–80 (2019).
29. Zanin, E. *et al.* Adsorption of heavy metals from wastewater graphic industry using clinoptilolite zeolite as adsorbent. *Process Saf. Environ. Prot.* **105**, 194–200 (2017).
30. Madondo, N. I. & Chetty, M. Aerobic co-digestion of sewage sludge and bio-based glycerol: Optimisation of process variables using one-factor-at-a-time (OFAT) and Box-Behnken Design (BBD) techniques. *S. Afr. J. Chem. Eng.* **40**, 87–99 (2022).
31. Xia, J. S., Ma, J. A. & Toghraie, D. Molecular dynamics simulation of friction process in atomic structures with spherical nanoparticles. *Solid State Commun.* **346**, 114717 (2022).
32. Shojaei, S., Shojaei, N., Nouri, A. & Baharinikoo, L. Application of chemometrics for modeling and optimization of ultrasound-assisted dispersive liquid-liquid microextraction for the simultaneous determination of dyes. *NPJ Clean Water* **4**(1), 1–8 (2021).
33. Nguyen, D. *et al.* Optimization of tetracycline adsorption onto zeolitic-imidazolate framework-based carbon using response surface methodology. *Surf. Interfaces* **28**, 101549 (2022).
34. Wang, J., Shojaei, S. & Shojaei, S. Removal of drug and dye from aqueous solutions by graphene oxide: Adsorption studies and chemometrics methods. *NPJ Clean Water* **5**(1), 1–10 (2022).
35. Shojaei, S. *et al.* Application of Taguchi method and response surface methodology into the removal of malachite green and pyramine-O by NaX nanozeolites. *Sci. Rep.* **11**(1), 1–13 (2021).
36. El-Ahmady El-Naggar, N., Rabei, N. H. & El-Malkey, S. E. Eco-friendly approach for biosorption of Pb²⁺ and carcinogenic Congo red dye from binary solution onto sustainable *Ulva lactuca* biomass. *Sci. Rep.* **10**(1), 1–22 (2020).
37. Masudi, A. *et al.* Equidistant crystal distortion arrangement of copper doped magnetite for paracetamol degradation and optimization with response surface methodology (RSM). *Mater. Chem. Phys.* **250**, 122995 (2020).
38. Venkata Rao, K. & Murthy, P. B. G. S. N. Modeling and optimization of tool vibration and surface roughness in boring of steel using RSM, ANN and SVM. *J. Intell. Manuf.* **29**(7), 1533–1543 (2018).
39. Bahrami, M. & Nezamzadeh-Ejhieh, A. Effect of supporting and hybridizing of FeO and ZnO semiconductors onto an Iranian clinoptilolite nano-particles and the effect of ZnO/FeO ratio in the solar photodegradation of fish ponds waste water. *Mater. Sci. Semicond. Process.* **27**, 833–840 (2014).
40. Treacy, M. M., Higgins, J. B. & von Ballmoos, R. *Collection of Simulated XRD Powder Patterns for Zeolites* Vol. 552 (Elsevier, 1996).
41. Bagheri, S., Esrafil, A., Kermani, M., Mehralipour, J. & Gholami, M. Performance evaluation of a novel rGO-FeO/Fe₃O₄-PEI nanocomposite for lead and cadmium removal from aqueous solutions. *J. Mol. Liq.* **320**, 114422 (2020).
42. Asfaram, A., Ghaedi, M., Agarwal, S., Tyagi, I. & Gupta, V. K. Removal of basic dye Auramine-O by ZnS:Cu nanoparticles loaded on activated carbon: Optimization of parameters using response surface methodology with central composite design. *RSC Adv.* **5**(24), 18438–18450 (2015).
43. Al Sadat Shafiof, M. & Nezamzadeh-Ejhieh, A. A comprehensive study on the removal of Cd(II) from aqueous solution on a novel pentetic acid-clinoptilolite nanoparticles adsorbent: Experimental design, kinetic and thermodynamic aspects. *Solid State Sci.* **99**, 106071 (2020).
44. Faghihian, H. & Nejati-Yazdinejad, M. Equilibrium study of the sorption of a sulphur-containing amino acid by clinoptilolite. *Adsorpt. Sci. Technol.* **27**(1), 19–29 (2009).
45. Cotton, A. Dissolution kinetics of clinoptilolite and heulandite in alkaline conditions. *Biosci. Horiz.* **1**(1), 38–43 (2008).
46. Palma-Anaya, E. *et al.* Pb(II) removal process in a packed column system with xanthation-modified deoiled allspice husk. *J. Chem.* **2017**, 1–8 (2017).

47. Shi, B., Zuo, W., Zhang, J., Tong, H. & Zhao, J. Removal of lead(II) ions from aqueous solution using *Jatropha curcas* L. seed husk ash as a biosorbent. *J. Environ. Qual.* **45**(3), 984–992 (2016).
48. Rahimi, S., Moattari, R. M., Rajabi, L., Derakhshan, A. A. & Keyhani, M. Iron oxide/hydroxide (α , γ -FeOOH) nanoparticles as high potential adsorbents for lead removal from polluted aquatic media. *J. Ind. Eng. Chem.* **23**, 33–43 (2015).
49. Chauhan, P., Bhasin, K. K. & Chaudhary, S. High selectivity and adsorption proficiency of surfactant-coated selenium nanoparticles for dye removal application. *Environ. Sci. Pollut. Res.* **28**(43), 61344–61359 (2021).
50. Awual, M. R. A facile composite material for enhanced cadmium(II) ion capturing from wastewater. *J. Environ. Chem. Eng.* **7**(5), 103378 (2019).
51. Khalifa, M. E., Abdelrahman, E. A., Hassanien, M. M. & Ibrahim, W. A. Application of mesoporous silica nanoparticles modified with dibenzoylmethane as a novel composite for efficient removal of Cd(II), Hg(II), and Cu(II) ions from aqueous media. *J. Inorg. Organomet. Polym. Mater.* **30**(6), 2182–2196 (2020).
52. Arabkhani, P. & Asfaram, A. Development of a novel three-dimensional magnetic polymer aerogel as an efficient adsorbent for malachite green removal. *J. Hazard. Mater.* **384**, 121394 (2020).
53. Shojaei, S., Shojaei, S. & Pirkamali, M. Application of Box-Behnken design approach for removal of acid black 26 from aqueous solution using zeolite: Modeling, optimization, and study of interactive variables. *Water Conserv. Sci. Eng.* **4**(1), 1–9 (2019).
54. Amani-Ghadim, A. R., Aber, S., Olad, A. & Ashassi-Sorkhabi, H. Optimization of electrocoagulation process for removal of an azo dye using response surface methodology and investigation on the occurrence of destructive side reactions. *Chem. Eng. Process.* **64**, 68–78 (2013).
55. Massoudinejad, M., Rasoulzadeh, H. & Ghaderpoori, M. Magnetic chitosan nanocomposite: Fabrication, properties, and optimization for adsorptive removal of crystal violet from aqueous solutions. *Carbohydr. Polym.* **206**, 844–853 (2019).
56. Nasab, S. G. *et al.* Decolorization of crystal violet from aqueous solutions by a novel adsorbent chitosan/nanodiopside using response surface methodology and artificial neural network-genetic algorithm. *Int. J. Biol. Macromol.* **174**, 429–443 (2019).
57. Shojaei, S., Ahmadi, J., Davoodabadi Farahani, M., Mehdizadehd, B. & Pirkamali, M. Removal of crystal violet using nanozeolite-x from aqueous solution: Central composite design optimization study. *J. Water Environ. Nanotechnol.* **4**(1), 40–47 (2019).
58. Khoshnamvand, N., Jafari, A., Kamarehie, B., Mohammadi, A. & Faraji, M. Removal of malachite green dye from aqueous solutions using zeolitic imidazole framework-8. *Environ. Process.* **6**(3), 757–772 (2019).
59. Shariifpour, E., Alipanhpour Dil, E., Asfaram, A., Ghaedi, M. & Goudarzi, A. Optimizing adsorptive removal of malachite green and methyl orange dyes from simulated wastewater by Mn-doped CuO-Nanoparticles loaded on activated carbon using CCD-RSM: Mechanism, regeneration, isotherm, kinetic, and thermodynamic studies. *Appl. Organomet. Chem.* **33**(3), e4768 (2019).
60. Ramezani, F. & Zare-Dorabei, R. Simultaneous ultrasonic-assisted removal of malachite green and methylene blue from aqueous solution by Zr-SBA-15. *Polyhedron* **166**, 153–161 (2019).
61. Singh, D. B., Rupainwar, D. C., Prasad, G. & Jayaprakas, K. C. Studies on the Cd(II) removal from water by adsorption. *J. Hazard. Mater.* **60**(1), 29–40 (1998).
62. Mansour, M. S., Ossman, M. E. & Farag, H. A. Removal of Cu(II) from waste water by adsorption onto polyaniline coated on sawdust. *Desalination* **272**(1–3), 301–305 (2011).
63. Jamil, T. S., Ibrahim, H. S., Abd El-Maksoud, I. H. & El-Wakeel, S. T. Application of zeolite prepared from Egyptian kaolin for removal of heavy metals: I. Optimum conditions. *Desalination* **258**(1–3), 34–40 (2010).
64. Li, W. *et al.* Tobacco stems as a low cost adsorbent for the removal of Pb(II) from wastewater: Equilibrium and kinetic studies. *Ind. Crops Prod.* **28**(3), 294–302 (2008).
65. El-Ashtouky, E. S., Amin, N. K. & Abdelwanis, O. Removal of lead(II) and copper(II) from aqueous solution using pomegranate peel as a new adsorbent. *Desalination* **223**(1–3), 162–173 (2008).
66. Zare, E. N., Lakouraj, M. M. & Karamian, N. Development of effective nano-biosorbent based on poly m-phenylenediamine grafted dextrin for removal of Pb(II) and methylene blue from water. *Carbohydr. Polym.* **201**, 539–548 (2018).

Acknowledgements

The research is supported by National Nature Science Foundation of China (Grant No. 41472325). Key projects of science and technology Department of Sichuan Province (20YYJC1188). Sichuan Education and teaching reform project (G2021-1070), the opening project of Sichuan province university key Laboratory (SC_FQWLY-2020-Z-02, 2020ZJ01) Zigong science and technology bureau project (2019RKX02).

Author contributions

X.S. and M.G.H. conceived and planned the experiments. I.P. and N.D. carried out the experiments, experimental design, and contributed to the interpretation of the results. K.U. performed SEM, XRD and BET analysis. H.J. and P.A. had a significant contribution for technical checking, validation and programming language checking and revision the manuscript in terms of grammar checking and writing. All authors discussed the results and contributed to the final manuscript.

Competing interests

The authors declare no competing interests.

Additional information

Supplementary Information The online version contains supplementary material available at <https://doi.org/10.1038/s41598-022-17636-8>.

Correspondence and requests for materials should be addressed to X.S. or M.G.

Reprints and permissions information is available at www.nature.com/reprints.

Publisher's note Springer Nature remains neutral with regard to jurisdictional claims in published maps and institutional affiliations.



Open Access This article is licensed under a Creative Commons Attribution 4.0 International License, which permits use, sharing, adaptation, distribution and reproduction in any medium or format, as long as you give appropriate credit to the original author(s) and the source, provide a link to the Creative Commons licence, and indicate if changes were made. The images or other third party material in this article are included in the article's Creative Commons licence, unless indicated otherwise in a credit line to the material. If material is not included in the article's Creative Commons licence and your intended use is not permitted by statutory regulation or exceeds the permitted use, you will need to obtain permission directly from the copyright holder. To view a copy of this licence, visit <http://creativecommons.org/licenses/by/4.0/>.

© The Author(s) 2022

RETRACTED ARTICLE